Chapter 5: EFFECT OF rGO-Ni CONTENT ON TRIBOLOGICAL BEHAVIOUR OF Ni ALLOY-BASED COMPOSITES

In Chapter 4, it was found that the addition of Ni-doped rGO imparts better tribological properties to Ni alloy-based composite in comparison to raw rGO. Therefore, it was thought to analyse the effect of the amount of Ni-doped rGO on the friction and wear performance of Ni alloy-based composites for determining the optimum content. This chapter presents the results on the microstructural characterization and tribological performance of the Ni alloy-based composites having fixed amount (10 wt.%) of Ag and different amounts (0.5, 1.0, 1.5, and 2.0 wt.%) of Ni-doped rGO, namely NANG0.5, NANG1.0, NANG1.5, and NANG2.0, respectively. The results have been discussed in light of the features observed on the worn surfaces of Ni alloy-based composites, and the counterface Si_3N_4 slid against them to develop an understanding of their tribological behaviour and to reveal the prevailing wear mechanisms.

5.1 RESULTS

5.1.1 Characterization of Composites

5.1.1.1 Morphology of ball-milled powders and composites

The fragmentation of flattened particles can be seen in milled powders for all as seen by a comparison of Figs. 5.1(a-d). The average size of flattened particles decreases from 61.5 to 29.9 μm with an increase in the amount from 0.5 to 2.0 wt.% of rGO.

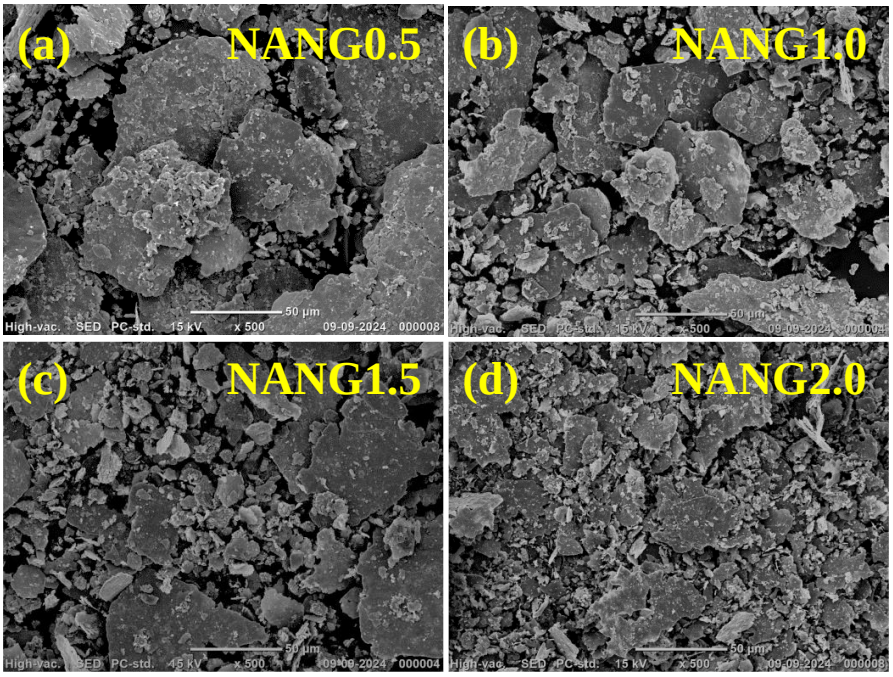

Fig. 5. 1 FESEM images of milled powders (a) NANG0.5, (b) NANG1.0, (c) NANG1.5, and (d) NANG2.0

The XRD patterns of the milled powders and sintered composites such NA, NANG0.5, NANG1.0, NANG1.5, and NANG2.0 have been shown in Fig. 5.2. The XRD patterns of both NA and NANG (renamed here as NANG1.0) which have also been presented in Chapter 4 are included again for the ready reference. The milled powder and sintered composites NA and NANG1.0 have shown the peaks pertaining to Ni, Cr, Mo, Ag, and MoC corresponding XRD patterns as discussed in Section 4.1.1.6. The milled powder of NANG0.5 exhibits peaks corresponding to Ni (ICSD 98-026-0169) at ~44.48 and 76.36º, Cr (ICSD 00-006-0694) at ~ 51.82, 64.52, 81.64, and 92.94º, Mo (ICSD 98-017-3127) at ~40.48, 58.64, and 73.78º, Ag (ICSD 01-087-0597) at ~38.10º, which are the major constituents of the composite. The milled powders of NANG1.5 and NANG2.0 show a similar pattern of peaks as observed for NANG0.5, along with additional peaks of rGO (ICSD 98-005-2916) at ~26.59º as seen in the inset of Fig. 5.2 (a). XRD pattern of the sintered composite NANG0.5 presents the peaks pertaining to Ni at 42.47, 45.21, and

76.52°, Cr at 49.80, 63.54, and 90.43°, Mo at ~74.24°, Ag at ~80.52° and MoC at ~37.03° as depicted in Fig. 5.2 (b). Similar peaks with additional peak of rGO at 26.90° have been observed for NANG1.5 and NANG2.0 in the XRD pattern, as seen in the XRD pattern of NANG0.5. The existence of elemental Ni, Cr, Mo, Ag, and rGO reveals that no oxidation took place during the sintering process in the inert atmosphere.

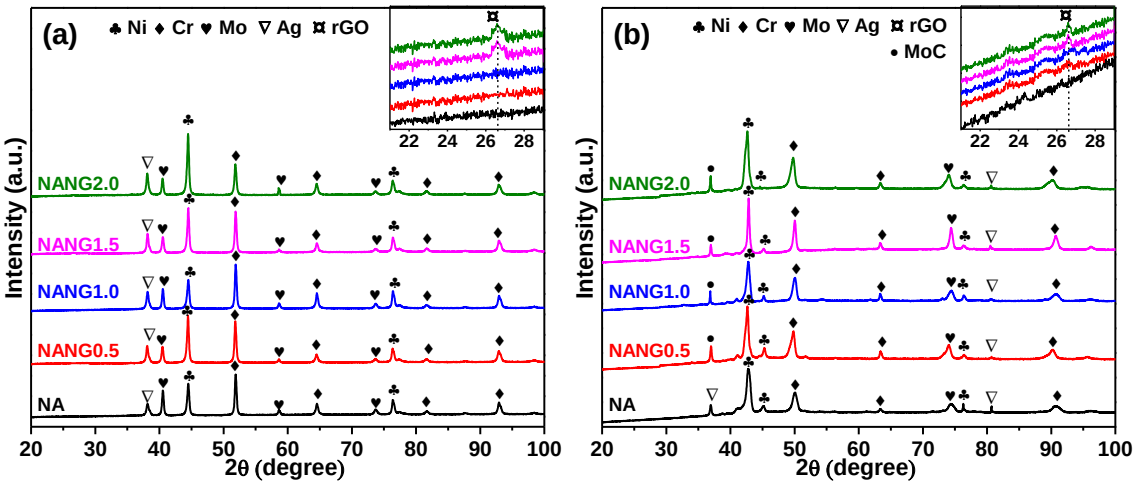

Fig. 5. 2 X-ray diffraction patterns of (a) ball milled powder and (b) spark plasma sintered composite for NA, NANG0.5, NANG1.0, NANG1.5, and NANG2.0

5.1.1.2 Microstructure of composites

The microstructure of the composites, i.e., NANG0.5, NANG1.0, NANG1.5, and NANG2.0, has been shown in Fig. 5.3. One may observe that the microstructure of NANG2.0 is much finer in comparison to others. EDS analysis of different regions (Figs. 5.3 (b and c)) has been given in Table 5.1. Region 1 of the NA reveals the existence of white spots (Ag-rich region) in the Ni-based solid solution. The presence of Ni-based solid solution (region 2) and light grey spots rich in Ag (region 3) have been observed for NA. However, some pores at different locations could also be seen in the microstructure of the composites containing rGO. The area elemental mapping for NANG0.5, NANG1.5, and

NANG2.0 has been depicted in Fig. 5.4. Since the same for NANG1.0 has been included in section 4.1.1.7, hence not shown here again. The analysis of the area elemental mapping of the composites suggests the homogenous distribution of the constituent elements in the matrix.

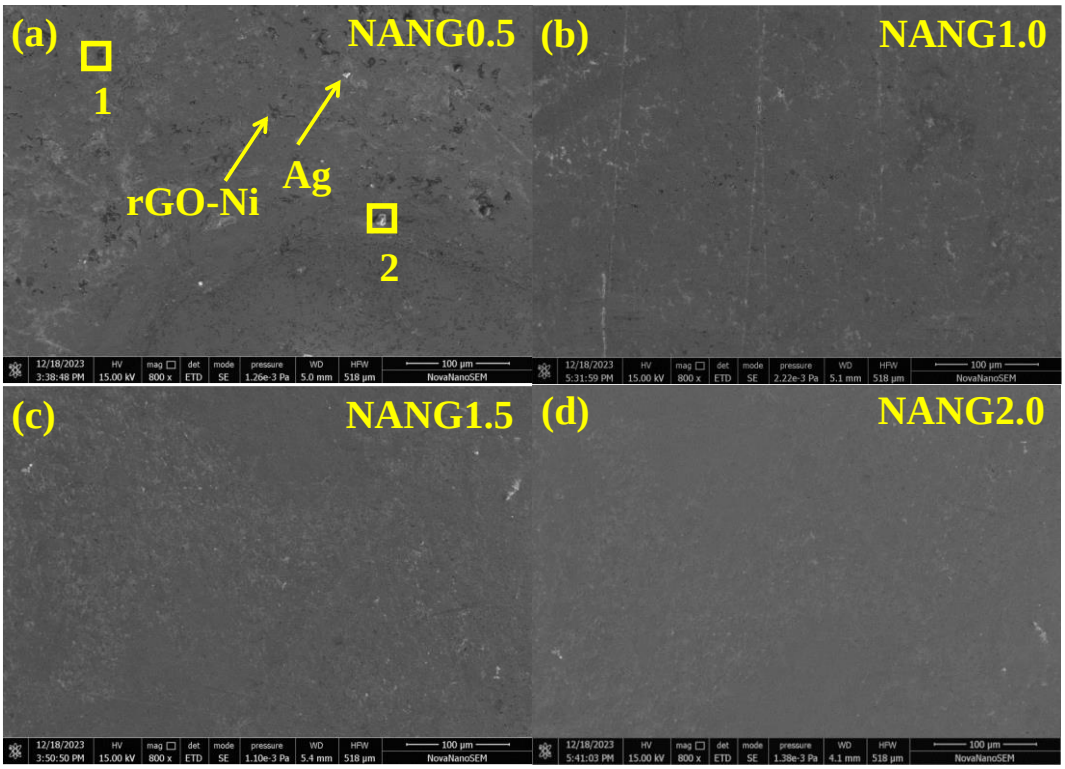

Fig. 5. 3 SEM micrographs of microstructure of (a) NANG0.5, (b) NANG1.0, (c) NANG1.5, and (d) NANG2.0

Table 5. 1 EDS analysis of marked regions in Fig. 5.3 (a)

Region	Element (wt.%)						
	Ni	Cr	Mo	Ti	Al	Ag	C
1	67.12	18.03	8.91	0.18	2.52	2.07	1.16
2	12.06	42.72	13.63	0.55	25.72	1.52	3.81

5.1.1.3 Hardness and density measurement of composites

The designation, composition, density and microhardness of the specimens are given in Table 5.2. The hardness of the base alloy (N0) has been found to decrease with the addition of 10 wt.% Ag (NA). However, the addition of rGO (0.5-2.0 wt.%) in NA results in an improvement in the hardness and 2.0 wt. % addition of rGO brings the hardness to approximately the same level of N0.

Table 5. 2 Specimen designation, composition, density, and microhardness

Designation	Composition	Real density (g/cm^3)	Microhardness $HV_{0.3}$ (GPa)
N0	Ni alloy	8.06	515 ± 5
NA	Ni alloy-10 wt.% Ag	8.46	496 ± 4
NANG0.5	Ni alloy-10 wt.% Ag- 0.5 wt.% rGO	7.69	500 ± 2
NANG1.0	Ni alloy-10 wt.% Ag- 1.0 wt.% rGO	7.77	510 ± 6
NANG1.5	Ni alloy-10 wt.% Ag-1.5 wt.% rGO	7.87	512 ± 2
NANG2.0	Ni alloy-10 wt.% Ag- 2.0 wt.% rGO	8.11	517 ± 1

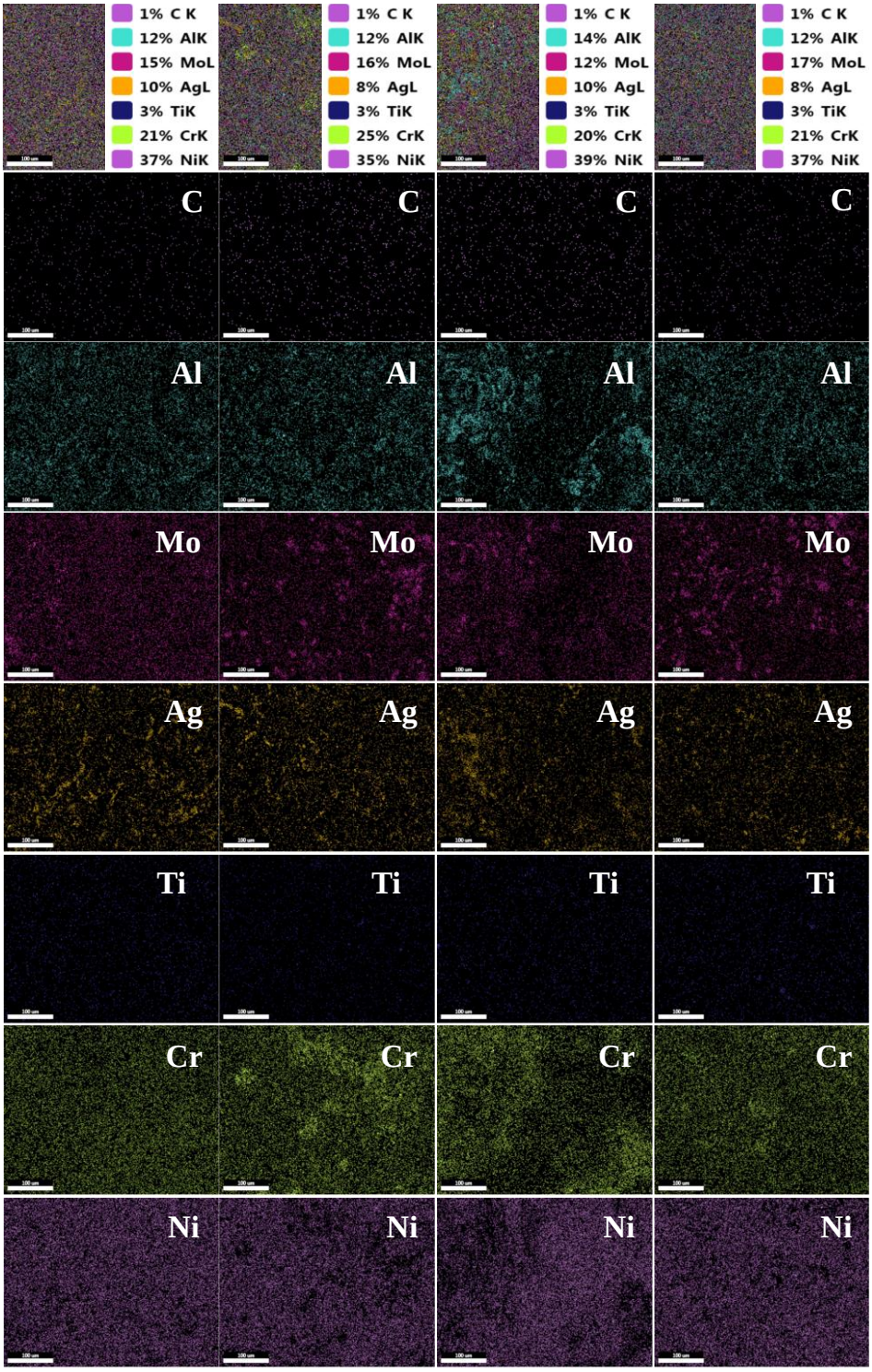

Fig. 5. 4 Area elemental mapping along with wt.% for (a) NANG0.5, (b) NANG1.0, (c) NANG1.5, and (d) NANG2.0

5.1.2 Dry Sliding Friction and Wear Behaviour

5.1.2.1 Variation of coefficient of friction with time

The variation in the coefficient of friction (CoF) with respect to time for base alloy (N0) and composites, i.e., NA, NANG0.5, NANG1.0, NANG1.5, and NANG2.0 at RT, 200, 400, 600, and 800 ºC at a fixed load and constant sliding speed as 5 N and 0.5 m/s, respectively, has been shown Fig. 5.5. All the samples exhibit a stable variation with only marginal fluctuations in amplitude after attaining the steady state at 200, 400, and 600 ºC in comparison to that of at RT and 800 ºC. The variation of CoF with time for N0 and NA at all the temperatures has been discussed in section 4.1.2.1.1, hence not included here. The CoF for NANG0.5, NANG1.0, NANG1.5, and NANG2.0 is found to stabilize at RT after 381, 180, 254, and 189 seconds, respectively, with relatively larger fluctuations in amplitude for NANG0.5 and NANG2.0 than NANG1.0 and NANG1.5 as shown in Fig. 5.5 (a). The CoF for NANG0.5, NANG1.0, NANG1.5, and NANG2.0 is found to stabilize at 200 ºC after 432, 192, 125, and 249 seconds, respectively, with relatively larger fluctuations in amplitude for NANG0.5 than others as seen from Fig. 5.5 (b). At 400 ºC, the CoF for NANG0.5, NANG1.0, NANG1.5, and NANG2.0 is observed to stabilize after 261, 520, 134, and 268 seconds, respectively, with relatively larger fluctuations in amplitude for NANG1.5 and NANG1.0 compared to NANG0.5 and NANG2.0 as depicted in Fig. 5.5 (c). At 600 ºC, the CoF for NANG0.5, NANG1.0, NANG1.5, and NANG2.0 stabilizes after 849, 410, 243, and 264 seconds, respectively, with greater fluctuations for NANG2.0 compared to others as seen from Fig. 5.5 (d). On the other hand, at 800 ºC, the CoF for NANG1.5 and NANG2.0 is found to stabilize after 153 and 132 seconds, respectively. However, both NANG0.5 and NANG1.0 have shown a slightly increasing trend of variation in CoF with duration of sliding as depicted in Fig. 5.5 (e).

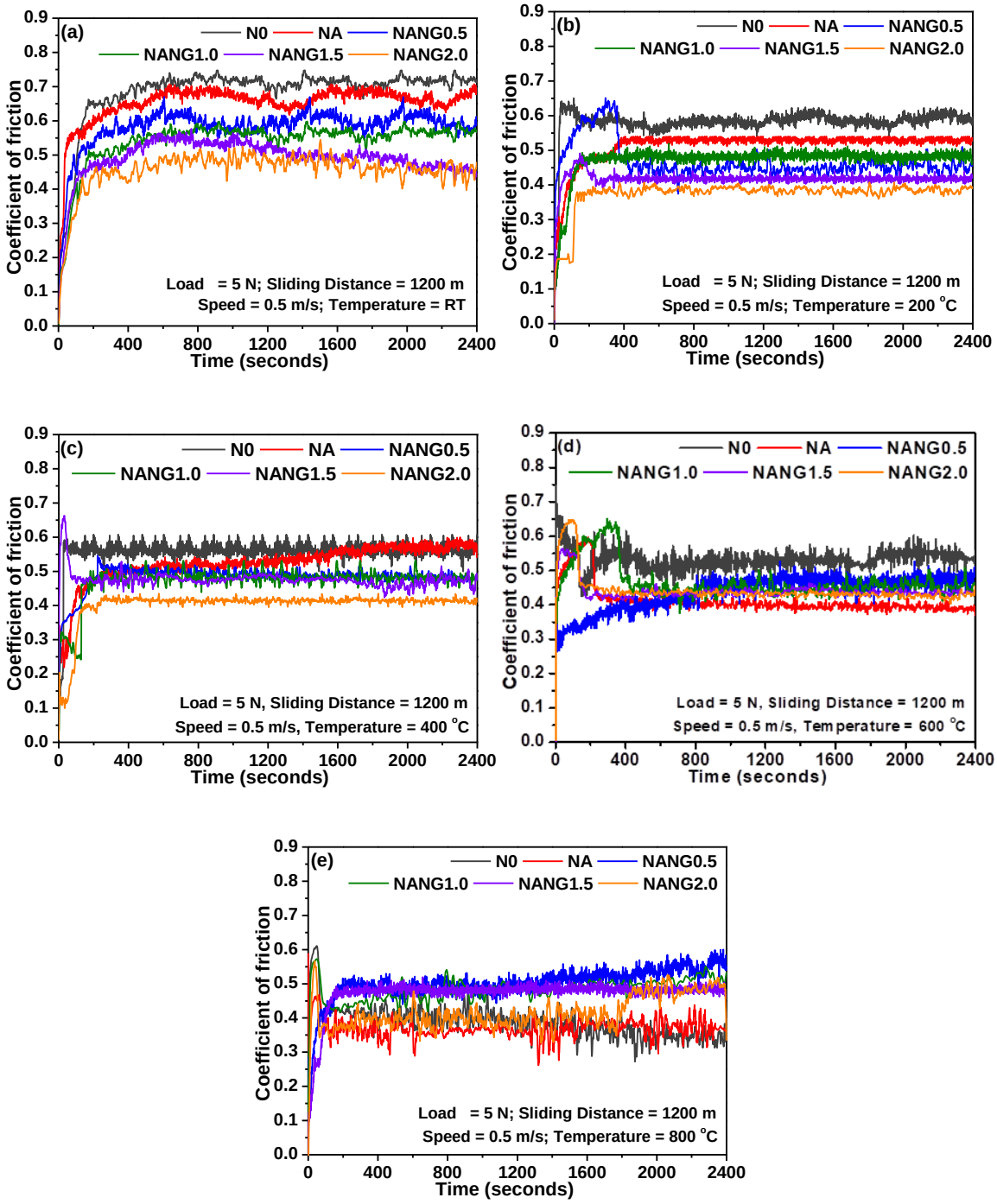

Fig. 5. 5 Variation of coefficient of friction with time at (a) RT, (b) 200, (c) 400, (d) 600, and (e) 800 °C for N0, NA, NANG0.5, NANG1.0, NANG1.5, and NANG2.0

5.1.2.2 Variation of average coefficient of friction with temperature

Figure 5.6 shows the variation of the average coefficient of friction (estimated by discarding the running-in period) with temperature for base alloy (N0) and composites, i.e., NA, NANG0.5, NANG1.0, NANG1.5, and NANG2.0. The average CoF for N0 and NA has been observed to decrease continuously from RT to 800 ºC with a significant decrease from RT to 200 ºC and 600 to 800 ºC. However, NA has shown a consistently lower CoF than N0 at all the temperatures. The CoF for NANG0.5 increases marginally from 200 to 400 ºC after a significant decrease from RT to 200 ºC, which is followed by a slight reduction from 400 to 600 ºC and an increase after that to 800ºC. A similar trend of variation CoF could be seen for NANG1.0 and NANG1.5. The CoF for NANG2.0 has been found to remain almost stable from 200 to 800 ºC after a decrease from RT to 200 ºC and it has exhibited the lowest CoF in comparison to other materials at all the temperatures except 800 ºC. The CoF of composites has been found to decrease with increasing amount of rGO-Ni at all the temperatures except 800 ºC.

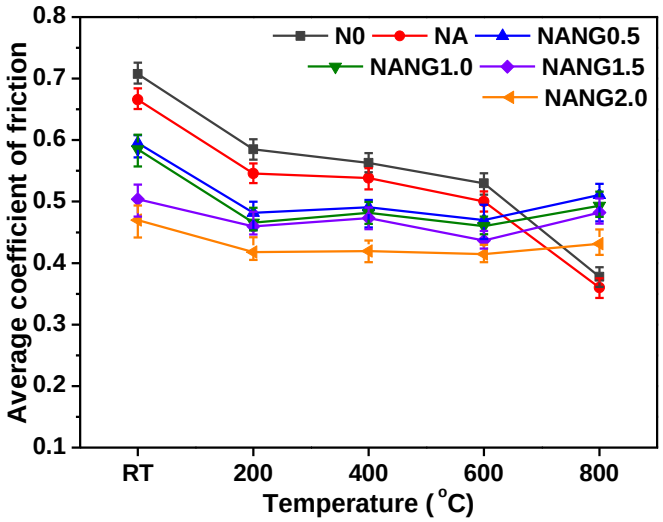

Fig. 5. 6 Variation of average coefficient of friction with temperature for the base alloy and composites

5.1.2.3 Variation of wear rate with temperature

The variation of specific wear rate (hereafter written as wear rate only) with temperature for all the samples has been depicted in Fig. 5.7. One may observe that the wear rate for N0 increases from RT to 600 ºC, which is followed by a sharp decrease afterward to 800 ºC. The wear rate for NA increases slightly from RT to 200 ºC, followed by a sharp increase up to 400 ºC and a decrease after that to 800 ºC. The wear rate for NANG0.5, NANG1.0, and NANG1.5 has been observed to increase marginally from RT to 200 ºC and then decrease to 600 ºC before increasing again to 800 ºC. However, the wear rate of NANG2.0 has been found to be almost the same from RT to 600 ºC with a slight decrease from 200 to 600 ºC, which is followed by a sharp increase to 800 ºC. It may be noted that the specific wear rate for the composites containing Ag and rGO decreases with an increase in the amount of rGO, and NANG2.0 has the lowest specific wear rate all the temperatures.

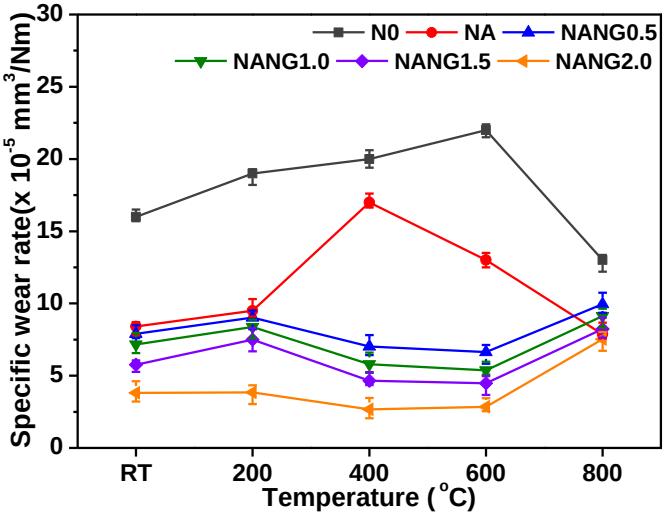

Fig. 5. 7 Variation of specific wear rate with temperature for the base alloy and composites

5.1.3 Analysis of Worn Surfaces

5.1.3.1 Electron microscopy of worn surfaces of tribo-pairs

The FESEM micrographs of the worn surfaces of NANG0.5 at RT, 200, 400, 600, and 800 ºC, along with their EDS analyses, are shown in Fig. 5.8 (a-j). The worn surface of NANG0.5 at RT (Fig. 5.8 (a)), shows the presence of shallow ploughing marks along with a transfer layer of wear debris, whereas the worn surface at 200 ºC (Fig. 5.8 (c)) exhibits the presence of some loose wear particles along with ploughing marks and delamination at few locations. The existence of wear debris, along with the transfer layer and delamination at a few places, could be observed on the worn surface (Figs. 5.8 (e and g)) at 400 and 600 ºC. However, a scattered transfer layer could be seen on the worn surface at 800 ºC as evident from Fig. 5.8 (i). EDS analyses of the square regions marked in Figs. 5.8 (a, c, e, g, and i) reveal the presence of constituent elements of the base alloy and oxygen along with their respective amounts depending on the temperature, indicating the possibility of oxidation as evident from EDS shown in Figs. 5.8 (b, d, f, h, and j).

The FESEM micrographs of the Si_3N_4 ball slid against NANG0.5 at RT, 200, 400, 600, and 800 ºC, along with the EDS analyses, are shown in Figs. 5.9 (a-j). The worn surface of the ball slid against NANG0.5 (Fig. 5.9 (a)) shows the existence of the transfer layers with varying degrees of compaction at RT, 200, 400, and 600 ºC as depicted in Figs. 5.9 (a, c, e, and g). One may observe a plateau of wear debris which appears to be spalling from the worn surface of the ball at 800 ºC as depicted in Fig. 5.9 (i). EDS analysis of the regions marked by squares on the worn surface of the ball given in Figs. 5.9 (b, d, f, h, and i) reveal the transfer of material from the composite to the ball, and the presence of oxygen points towards the oxidation of elements.

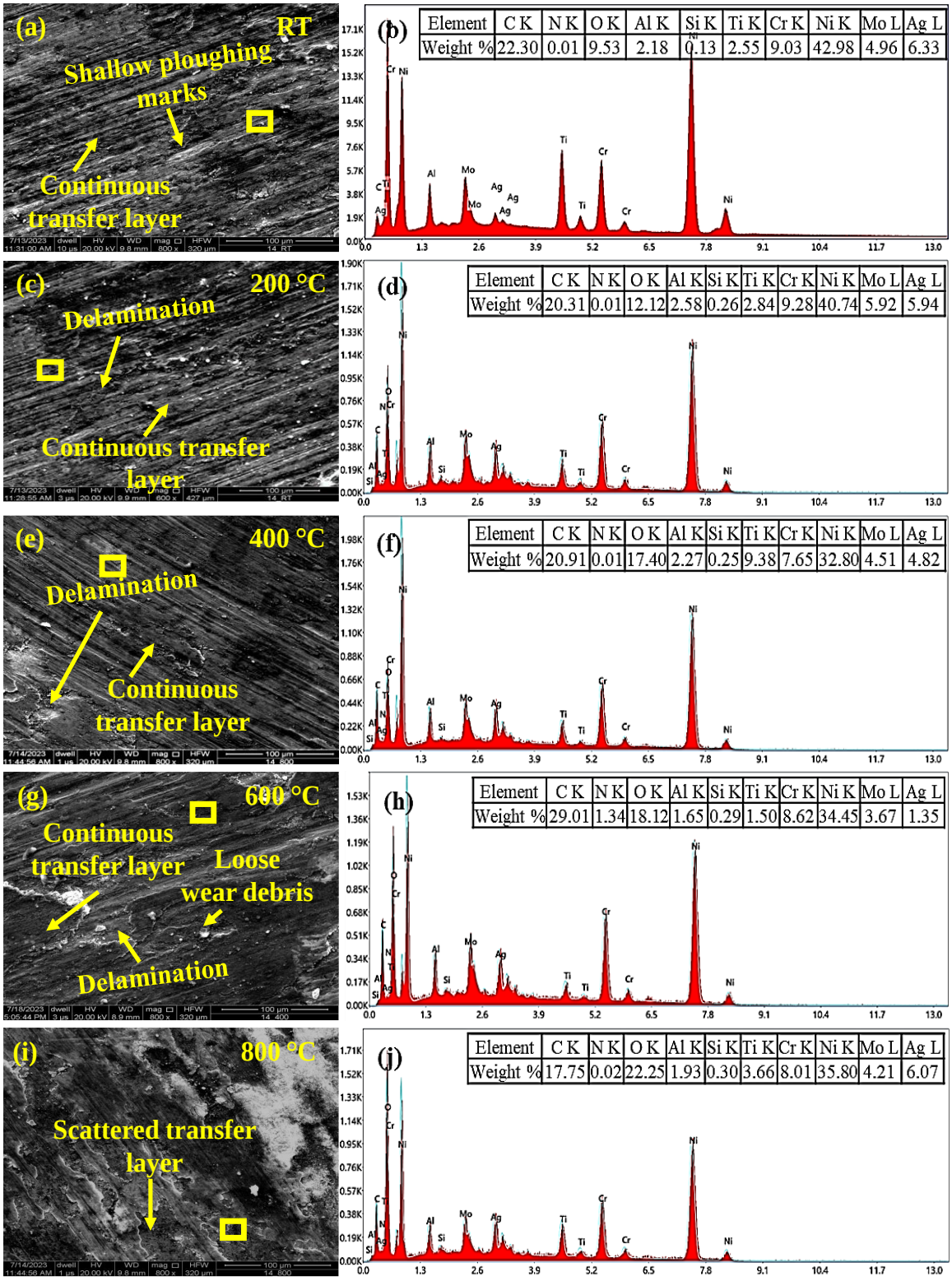

Fig. 5. 8 FESEM micrographs of the worn-out NANG0.5 and EDS of the marked region at (a and b) RT, (c and d) 200, (e and f) 400, (g and h) 600, and (i and j) 800 °C

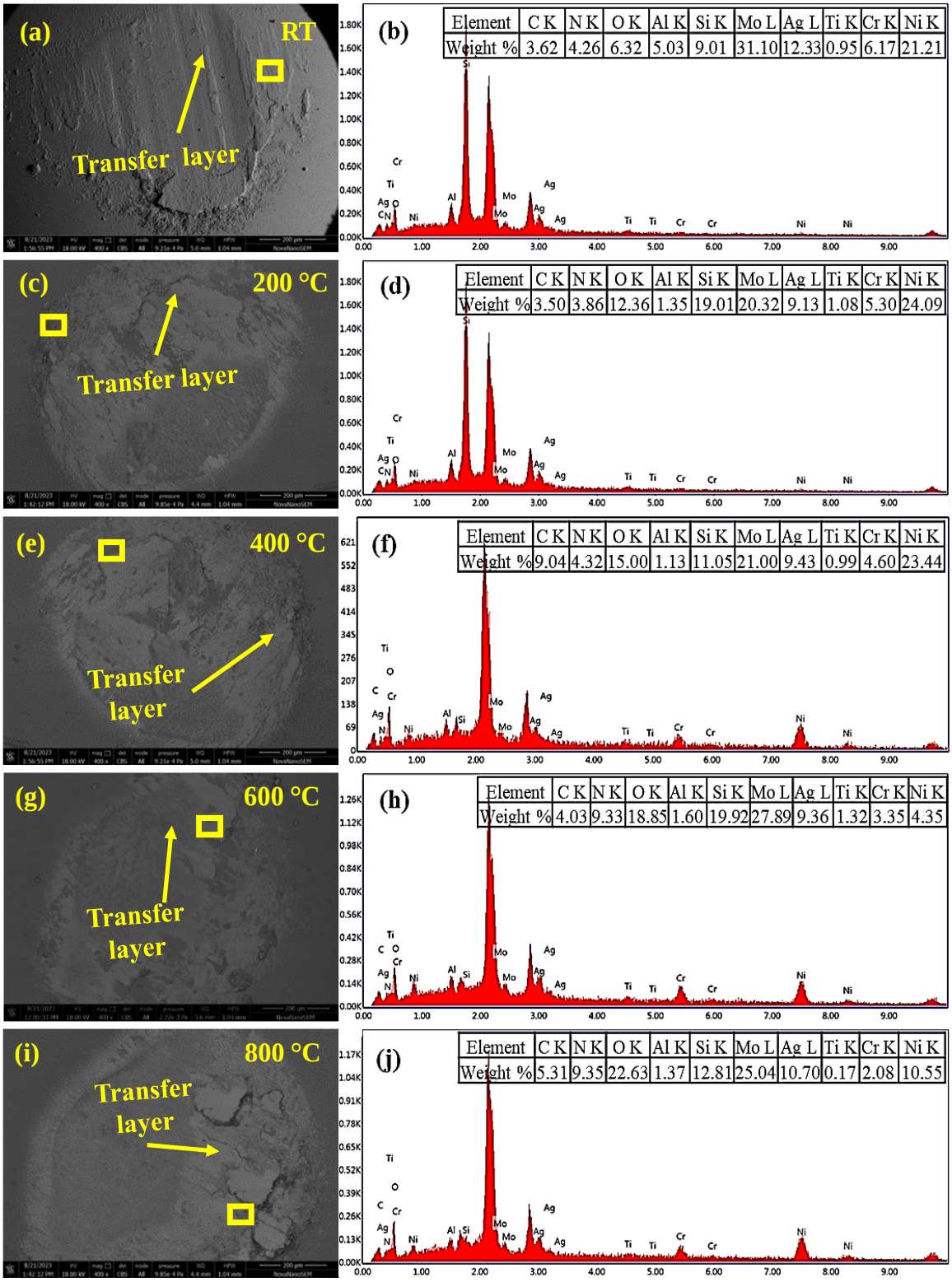

Fig. 5. 9 FESEM micrographs of the worn-out silicon nitride ball (counterface) slid against NANG0.5 along with EDS at the marked region at (a and b) RT, (c and d) 200, (e and f) 400, (g and h) 600, and (i and j) 800 °C

The morphological analysis of the worn surfaces of NANG1.0 has already been provided in detail in Chapter 4, hence not included here. Figures 5.10 (a-j) illustrate the morphology of the worn surfaces of the NANG1.5 after the tribo-tests at RT, 200, 400, 600, and 800 ºC, along with their EDS analyses. The worn surface morphology of NANG1.5 at RT (Fig. 5.10 (a)) shows the presence of shallow ploughing marks along with a continuous transfer layer, whereas the worn surface at 200 ºC (Fig. 5.10 (c)) reveals the presence of a relatively deeper ploughing marks along with the transfer layer and signs of its delamination at some locations. The existence of a continuous transfer layer with some delamination at a few locations could also be observed on the worn surface of NANG1.5 at 400 ºC (Fig. 5.10 (e)). The worn surface at 600 ºC reveals the presence of a relatively compact and continuous transfer layer compared to that observed at 400 ºC as seen from Figs. 5.10 (e and g). However, a scattered transfer layer and some loose wear debris are the visible features on the surface worn at 800 ºC. EDS analyses of the square regions marked in Figs. 5.10 (a, c, e, g, and i) show the existence of constituent elements of the composite and oxygen along with their respective amounts depending on the temperature, indicating the possibility of oxidation as evident from EDS shown in Figs. 5.10 (b, d, f, h, and j).

The FESEM micrographs of the Si_3N_4 ball slid against NANG1.5 at RT, 200, 400, 600, and 800 ºC, along with the EDS analyses, are shown in Figs. 5.11 (a-j). The accumulation of the wear debris can be seen at the leading edge of the worn surface of the ball slid against NANG1.5 at RT (Fig. 5.11 (a)). The worn surfaces of the ball slid at 200 and 400 ºC reveal the presence of a plateau of wear debris as observed in Figs. 5.11 (c and e). A smooth and scattered transfer layer covering a larger area of the surface can be seen for the ball worn at 600 ºC (Fig. 5.11 (g)). However, a relatively more compact transfer layer covering relatively smaller area and delamination at a few locations could be seen on the worn surface of the ball at 800 ºC (Fig. 5.11 (i)). EDS analysis of the regions marked by squares on the worn surface of the ball given in Figs. 5.11 (b, d, f, h, and i) reveal the transfer of material from the composite to the ball, and the presence of oxygen points towards the oxidation of elements.

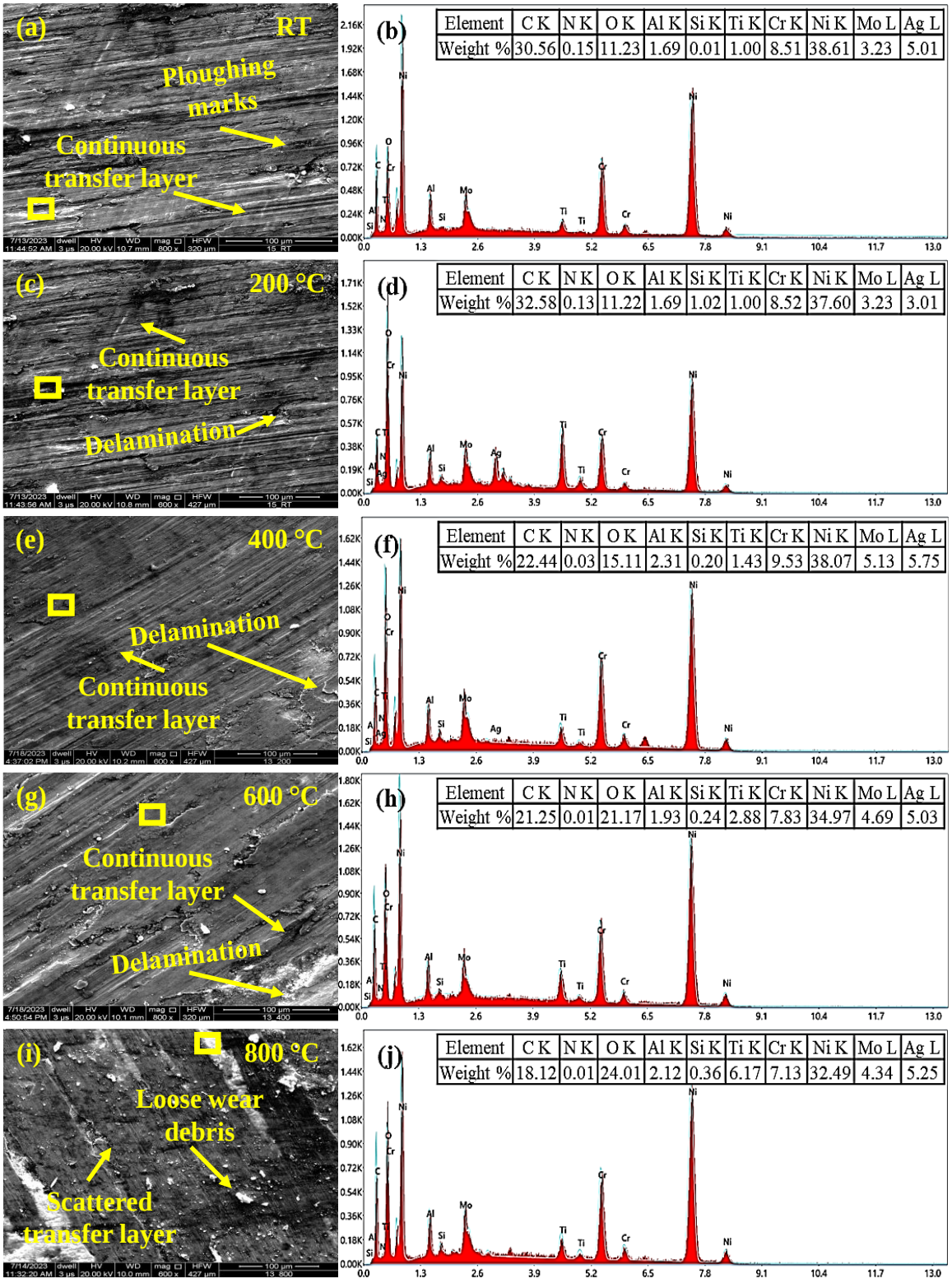

Fig. 5. 10 FESEM micrographs of the worn-out NANG1.5 and EDS of the marked region at (a and b) RT, (c and d) 200, (e and f) 400, (g and h) 600, and (i and j) 800 °C

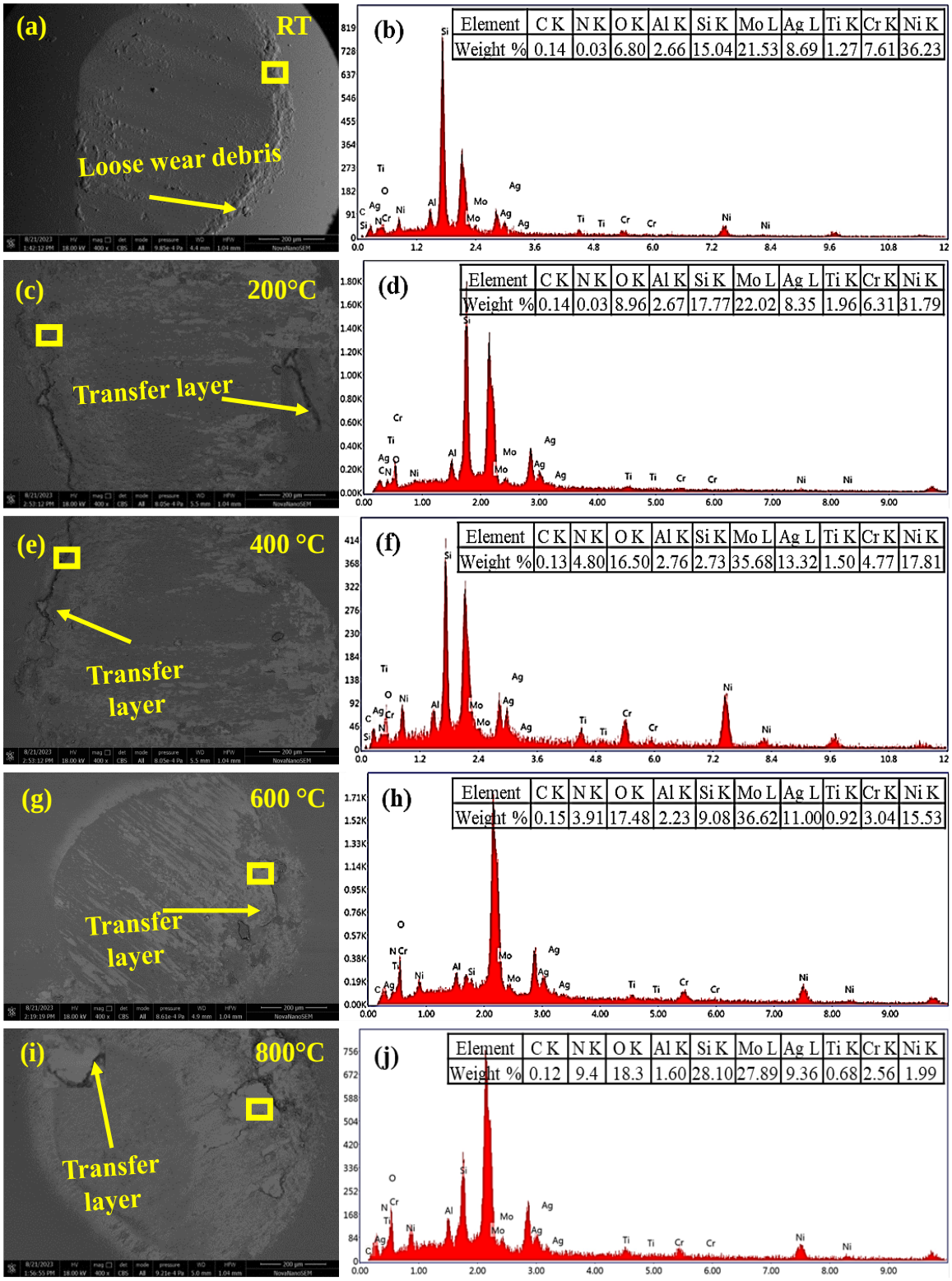

Fig. 5. 11 FESEM micrographs of the worn-out silicon nitride ball (counterface) slid against NANG1.5 along with EDS at the marked region at (a and b) RT, (c and d) 200, (e and f) 400, (g and h) 600, and (i and j) 800 °C

The FESEM images of the worn surfaces of the NANG2.0 and counterface ball at RT, 200, 400, 600, and 800 ºC, along with their EDS analyses, are depicted in Figs. 5.12 (a–j). The presence of a transfer layer and ploughing marks can be seen on the surface of NANG2.0 worn at RT as shown in Fig. 5.12 (a). The relatively fine ploughing marks along with a transfer layer covering almost the entire area, can be observed on the worn surface, at 200 ºC as compared to RT as seen from Figs. 5.12 (a and c). The presence of a continuous transfer layer with fine ploughing marks can be observed on the worn surface NANG2.0 at 400 and 600 ºC as illustrated in Figs. 5.12 (e and g). At 800 ºC, the worn surface of NANG2.0 reveals the existence of a scattered transfer layer with loose wear particles and delamination at a few places, as evident from Fig. 5.12 (i). Again, the EDS analyses of the square regions marked on the worn surface of NANG2.0 as shown in Figs. 5.12 (a, c, e, g, and i) have revealed the presence of constituent elements of the composite and oxygen as evident from Fig. 5.12 (b, d, f, h, and j).

The FESEM micrographs of the Si_3N_4 ball slid against NANG2.0 along with their EDS analyses at RT, 200, 400, 600, and 800 ºC are shown in Figs. 5.13 (a-j). At RT, the worn surface of the ball slid against NANG2.0 shows the presence of a well-compacted transfer layer with a very small area coverage as seen from Fig. 5.13 (a), whereas a relatively compact transfer layer covering a larger area could be observed at 200 ºC as seen from Fig. 5.13 (c). The transfer layer on the worn surface of the ball at 400 ºC appears to be more compact and has a larger coverage area compared to that seen at 200 ºC as evident from Figs. 5.13 (c and e). The worn surfaces of the ball slid against NANG2.0 at 600 and 800 ºC also reveal the presence of transfer layers with different features. The layer appears to be smooth with a full area coverage of the surface at 600 ºC and some locations of detachment (Fig. 5.13 (g)), while at 800 ºC the transfer layer is a bit thicker and seems to be at the verge spalling at the edge of the ball as depicted in Figs. 5.13 (g and i). EDS analyses of the regions marked by squares on the worn surface of the ball given in Figs. 5.13 (b, d, f, h, and i) reveal the transfer of material from the composite to the ball, and the presence of oxygen points towards the oxidation of elements.

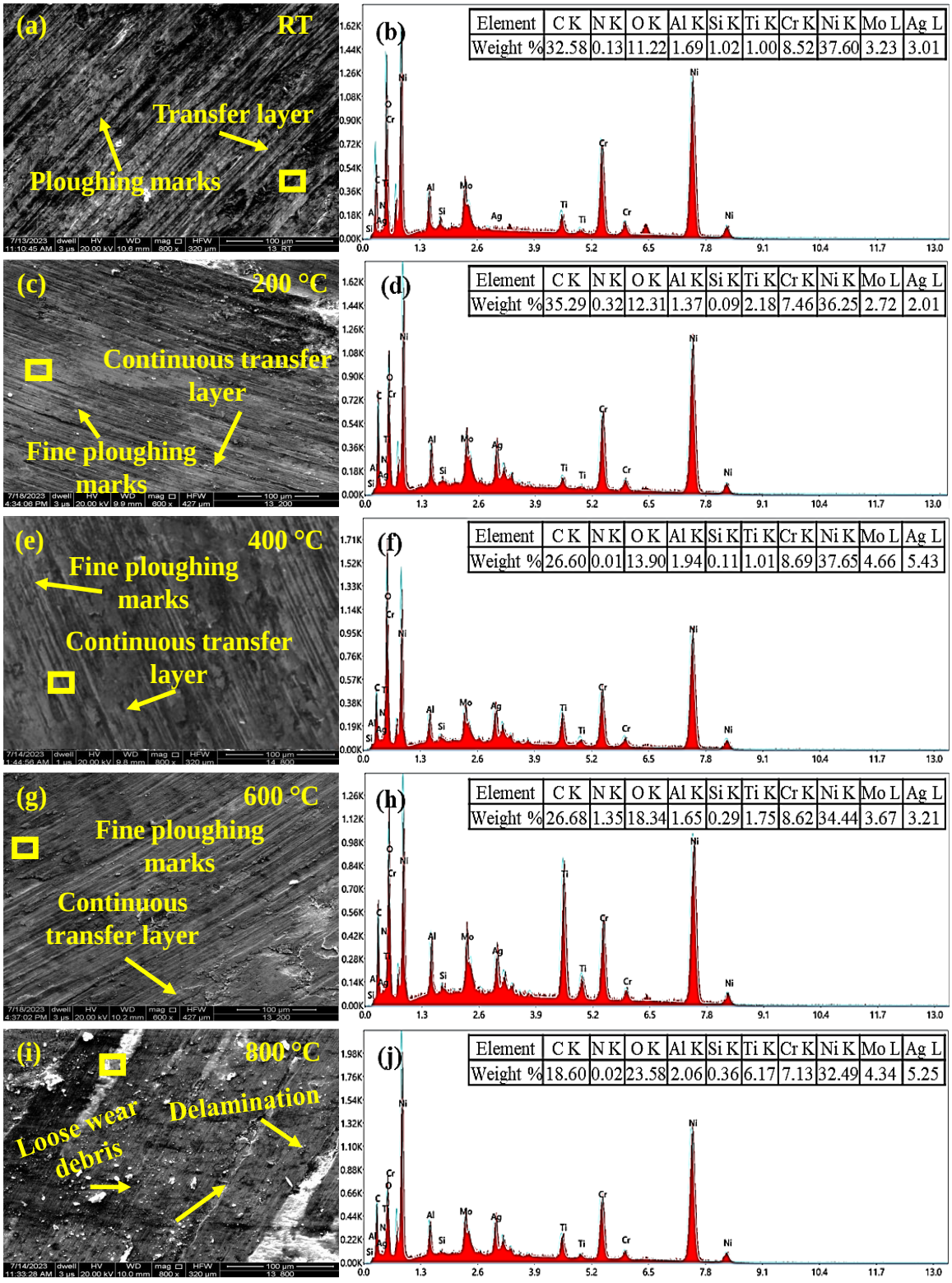

Fig. 5. 12 FESEM micrographs of the worn-out NANG2.0 and EDS of the marked region at (a and b) RT, (c and d) 200, (e and f) 400, (g and h) 600, and (i and j) 800 °C

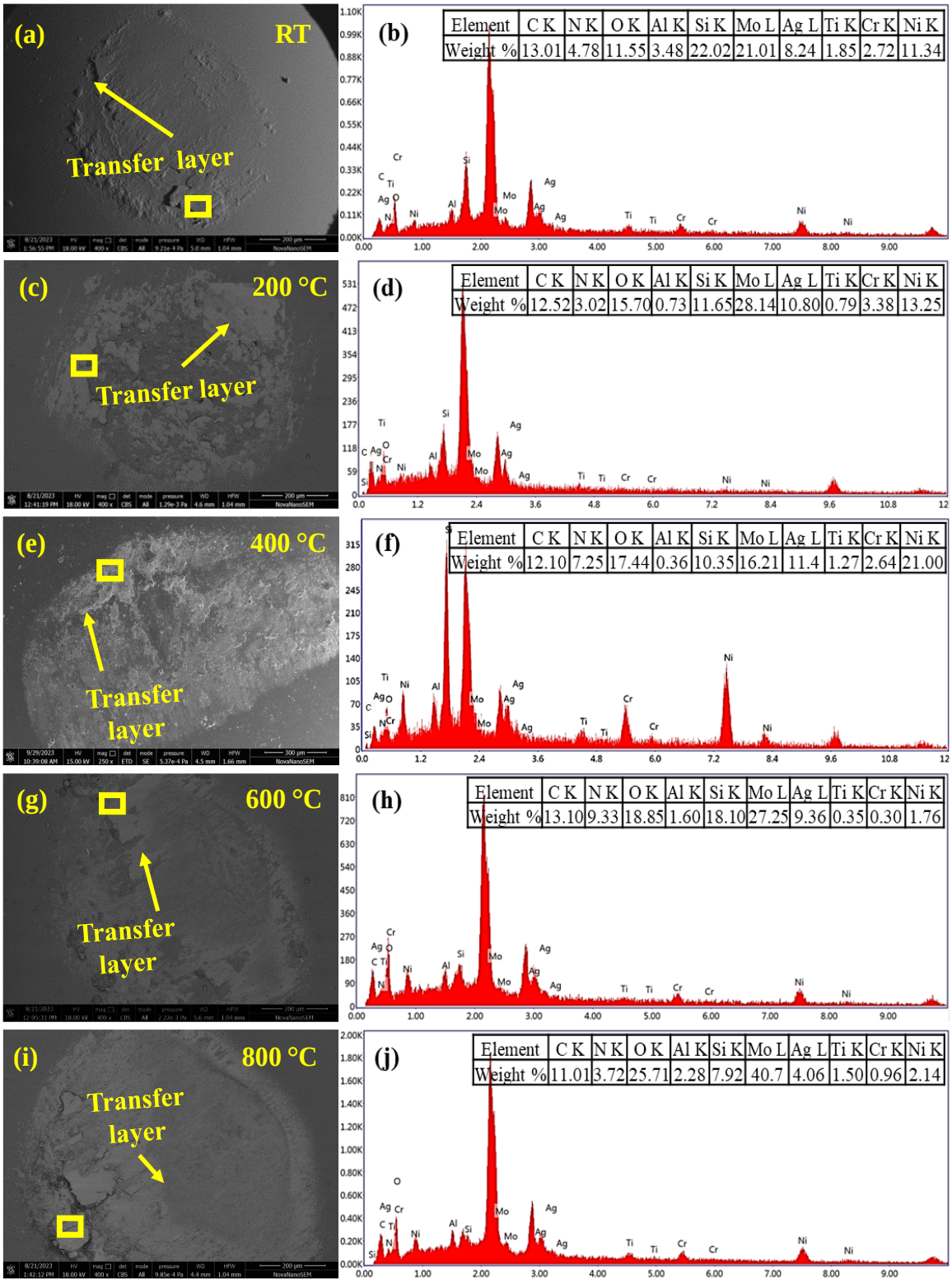

Fig. 5. 13 FESEM micrographs of the worn-out silicon nitride ball (counterface) slid against NANG2.0 along with EDS at the marked region at (a and b) RT, (c and d) 200, (e and f) 400, (g and h) 600, and (i and j) 800 °C

5.1.3.2 X-ray diffraction analysis of the worn surface of composites

The X-ray diffraction patterns of the worn surface of NANG0.5, NANG1.5, and NANG2.0 at RT, 200, 400, 600, and 800 ºC, are given in Fig. 5.14. XRD pattern for NANG 1.0 has already been presented and discussed in Section 4.1.3.2, so it is not included here. The XRD pattern of the worn surface of NANG0.5 (Fig. 5.14 (a)) reveals the presence of diffraction peaks corresponding to Ag (ICSD 01-087-0598), NiCr (ICSD 98-010-2819), NiAl (ICSD 98-060-4356), NiTi (ICSD 98-016-6010), Ni_6Mo_6C (ICSD 98-061-8328), and MoC (ICSD 98-004-3523) at RT, while a new peak of $Cr_{23}C_6$ (ICSD 98-006-2667) could be observed at 200 ºC. The additional peaks corresponding to NiO (ICSD 98-009-2129), MoO_3 (ICSD 00-021-0569), and $Ag_3Ni_2O_4$ (ICSD 98-017-2878) could be seen at 400 ºC. However, the presence of peaks pertaining to $Ag_2Mo_2O_7$ (ICSD 00-021-1339) and $NiMoO_4$ (ICSD 98-017-4488) could be observed at 600 and 800 ºC. XRD pattern of the worn surface of NANG1.5 and NANG2.0 have revealed the presence of peaks similar to those observed for NANG0.5 at all temperatures except the peaks corresponding to Ag_2MoO_4 (ICSD 00-008-473) and $NiMoO_4$ at 400, 600, and 800 ºC as seen from Figs. 5.14 (b and c).

5.1.3.3 Examination of Subsurface

FESEM images of the cross-section of the surfaces of nanocomposites, i.e., NANG0.5, NANG1.5, and NANG2.0, worn at 800°C as shown in Figs. 5.15 (a-c) confirm the presence of a tribo-layer. The average thickness of the tribo-layer for NANG0.5, NANG1.5, and NANG2.0 has been observed to be 33.4, 79.8, and 108.3 μm, respectively.

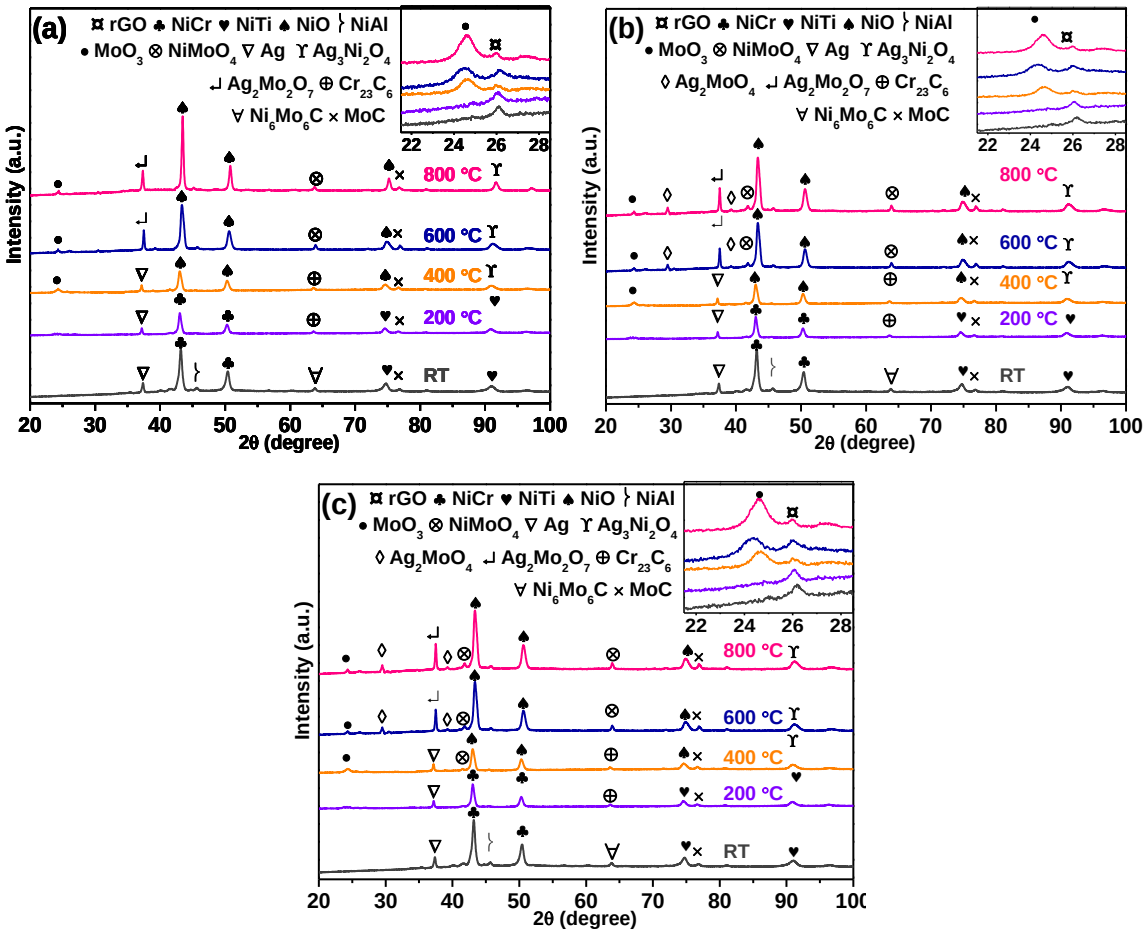

Fig. 5. 14 X-ray diffraction patterns of worn composite (a) NANG0.5, (b) NANG1.5, and (c) NANG2.0 at various temperatures

5.2 DISCUSSION

A reduction in the hardness of base alloy (N0) with the incorporation of silver is credited to the inherent softness of Ag, which has also been stated by other researchers [39,67]. However, the addition of a combination of Ag and rGO brings the hardness to the same level of N0 as seen from Table 5.2. The increase in the hardness of NA with an increase in the amount of rGO from 0.5 to 2.0 wt. % can be attributed to the hard nature of rGO as reported by other researchers [98,99]. Another contributing factor may be the enhanced wettability of rGO due to its doping by Nickel.

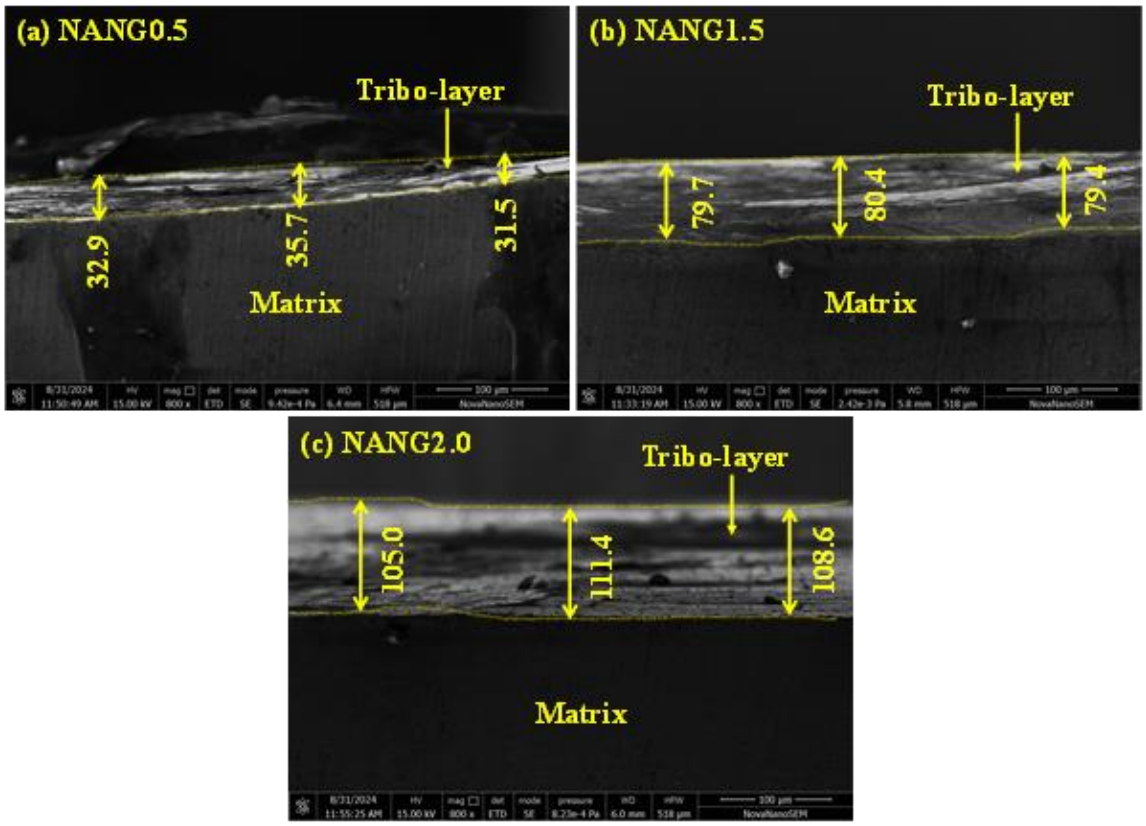

Fig. 5. 15 FESEM micrographs of cross-section of subsurface of worn track at 800 °C corresponding to (a) NANG0.5, (b) NANG1.5, and (c) NANG2.0

The initial fluctuations and subsequent stabilization of CoF with time at different temperatures as seen in Fig. 5.5, can be attributed to the deformation of the asperities and attainment of conformity with the progression of sliding. The observed friction and wear behaviour for the composites (Figs. 5.6 and 5.7) can be elucidated on the basis of the various events occurring during the sliding process as depicted in Fig. 5.16 depending on the composition and temperature. The presence of loose wear debris causes abrasion [65,67,94], leading to relatively higher friction and higher loss of material, whereas the formation of a transfer layer of wear debris inhibits the direct contact between the mating bodies with an attendant reduction in both the CoF and the material loss depending on its nature and the coverage over the worn surface. A continuous and well-compacted layer covering a greater area of the surface provides an effective hindrance to the direct contact

between the tribo-pair in comparison to the one which is scattered, loosely bound, and covers a relatively lesser area. The presence of lubricious species in the transfer layer also helps in diminishing the friction and material loss by providing a low shearing interface between the mating materials.

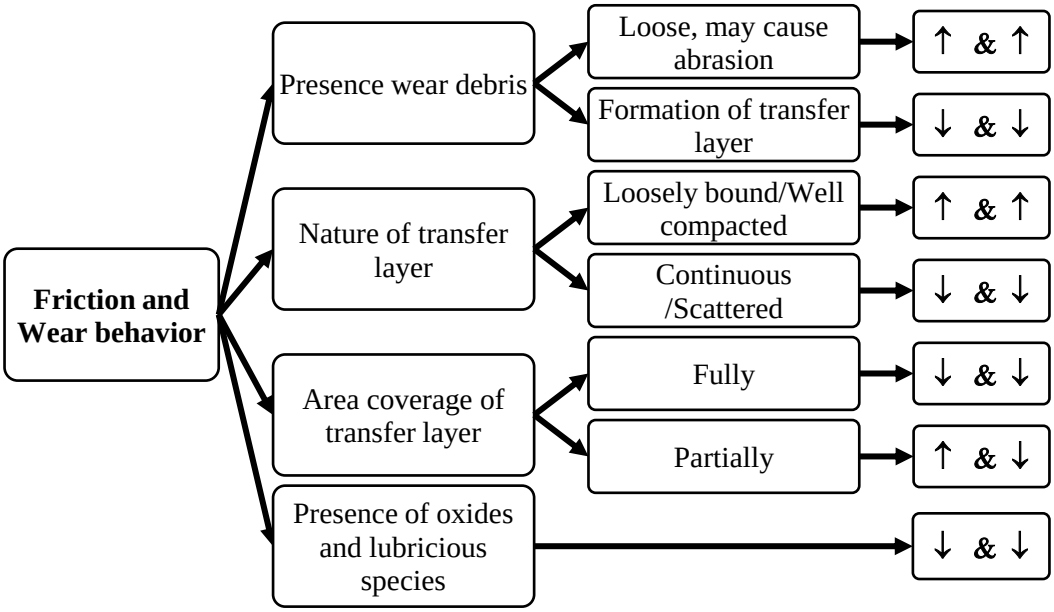

Fig. 5. 16 Features on the worn surface affecting the friction and wear behaviour under dry sliding

The observed variation of average CoF with temperature for both NA and N0 has already been discussed in our earlier published work [100] on the basis of the features present on their worn surfaces, such as the existence of loose wear particles, the nature of the transfer layer and its delamination, the presence of lubricious species, the X-ray diffraction, and the Raman spectroscopy depending on the test temperature. Hence, details are not provided here. Based on the morphology of the worn surface, the wear mechanisms for N0 and NA have been found to be ploughing and delamination from RT to 400 ºC, which changes to oxidative wear at 600 and 800 ºC.

A decrease in CoF from RT to 200 ºC for NANG0.5 as seen from Fig. 5.5 may be credited to the reduction in the depth of ploughing marks as well as the presence of the

transfer layer, which may have a relatively larger amount of Ag due to increased diffusion at 200 ºC. Moreover, the area coverage by the transfer layer on the worn surface of NANG0.5 and the corresponding ball appears to be relatively more at 200 ºC than at RT as seen from a comparison of Figs. 5.8 (a and c) and Figs. 5.9 (a and c), respectively, which might also have contributed in reducing CoF. A marginal increase in CoF of NANG0.5 from 200 to 400 ºC followed by a slight decrease at 600 ºC (Fig. 5.6) may be explained on the basis of the morphology of the worn surfaces of tribo-pair at these temperatures, which present almost similar features such as the presence of continuous transfer layer, loose wear particles and some locations of delamination with slight variation in their characteristics as evident from Figs. 5.8 (c, e, and g) and Figs. 5.9 (c, e, and g). The presence of lubricious species ($Ag_2Mo_2O_7$, NiO, $NiMoO_4$, MoO_3, and rGO) on the worn surface of composite as reflected by EDS spectrums depicted in Figs. 5.8 (b, d, f, and h) and confirmed by XRD analysis (Fig. 5.14 (a)) and the presence of transferred elements along with oxygen on the worn surface of ball as indicated by the EDS spectrums given in Figs. 5.8 (b, d, f, and h) might have also contributed to a decrease in CoF with increasing temperature. The lubricious species endow the surface with easy shearing capability leading to a reduction in CoF. The other contributing factor may be the synergistic action between Ag and rGO, which help in supplementing each other's lubricating capability by overcoming the drawbacks of employing a single solid lubricant. An increase in CoF at 800 ºC might be due to the presence of a scattered transfer layer on the worn surfaces of tribo-pair covering a relatively lesser area of the worn surface in comparison to that at 600 ºC as evident from a comparison of Figs. 5.8 (g and i) and Figs. 5.9 (g and i), which might have given rise to a direct contact between mating bodies, leading to an increase in CoF despite the presence of lubricious compounds. The variation of CoF with temperature for composites NANG1.0, NANG1.5, and NANG2.0 may again be explained on similar lines based on the morphological features seen on the worn surface of these composites and the counterface slid against them as shown in Figs. 5.10-5.13 depending on temperature and their relative

dominance. The decrease in CoF of the composites containing Ag and rGO with increasing amounts of rGO may be attributed to the presence of a relatively larger amount of lubricating agent, i.e., rGO, apart from the increasing hardness with an increasing amount of rGO as seen from Table 5.2. Hence, NANG2.0 has the lowest CoF, and NANG0.5 has the highest at all the temperatures.

The increase in the wear rate of NANG0.5 (Fig. 5.7) from RT 200 ºC may be attributed to the regions of delamination of the transfer layer present over the worn surface at 200 ºC as compared to RT, which do not show any delamination (Figs. 5.8 (a and c)) leading to a relatively larger loss of material due to direct contact between the mating bodies. However, a decrease in wear rate from 200 to 400 ºC may be credited to the presence of a relatively compact transfer layer on the worn surfaces of tribo-pairs as seen from Figs. 5.8 (c and e) and Figs. 5.9 (c and e), which effectively shields the specimen from coming in direct contact with the counterface ball, resulting in reduced wear rate. The other contribution comes from an increased presence of lubricating species at relatively higher temperatures, which offers low shearing ability at the interface and helps in reducing wear loss. A marginal decrease in wear rate for NANG0.5 from 400 to 600 ºC may be explained with the help of similar features present over the worn surfaces of tribo-pair at these temperatures as depicted in Figs. 5.8 (e and g) and Figs. 5.9 (e and g). However, an increase in wear rate at 800 ºC may be ascribed to the presence of a scattered transfer layer covering a relatively smaller area of the worn surface compared to that at 600 ºC as confirmed from a comparison of Figs. 5.8 (g and i), which allows direct contact between mating bodies, leading to an increase in material loss despite the existence of lubricious compounds. The softening of the surface at relatively higher temperatures may also have contributed in increasing the wear rate at 800 ºC as reported by other researchers [101,102]. A similar explanation would also suffice for the variation of wear rate with temperature for other composites NANG1.0, NANG1.5, and NANG2.0 based on the characteristic features

observed on the worn surfaces of composites as well as their respective counterparts shown Figs. 5.10-5.13. The decreasing wear rate of the composites containing increasing amount of rGO may be credited to the presence of its comparatively larger amount available for lubrication in addition to the increased hardness with increasing rGO. The same may also be confirmed based on the observed thickness of tribo-layer over the worn surface of NANG0.5, NANG1.0, NANG1.5, and NANG2.0 as illustrated in Fig. 5.15, which reveals that the thickness increases with increasing amount of rGO.

The dominant wear mechanisms for NANG0.5, NANG1.0, and NANG1.5 are ploughing and delamination from RT to 200ºC, delamination at 400ºC and a combination of abrasion and oxidation at 600 and 800ºC as revealed by the worn surface morphologies at these temperatures. However, the wear mechanism for NANG2.0 is a combination of ploughing and abrasion from RT to 600ºC, whereas the same is oxidative at 800 ºC.

To summarize, the composite containing 2.0 wt. % rGO, i.e., NANG2.0 has shown the lowest CoF and wear rate among all the materials at temperatures from RT to 600 ºC, which reflects the cooperative synergy between Ag and rGO in attaining low friction and wear over this range of temperature. The wear rate shown by NANG2.0 is approximately the same as that of NA at 800 ºC despite the presence of rGO which indicates the probable loss of assistive action between Ag and rGO at this temperature. The other factor may be the difference in tribo-layer thickness as explained above. On the basis of the above, one may conclude that a synergetic action between Ag and rGO occurs from RT to 600 ºC, which diminishes both the friction and the wear rate by overcoming the impediments of employing a single solid lubricant at a comparable level of hardness of the base alloy.